Discovery of a dihydroisoquinolinone derivative (NVP-CGM097) – a highly potent and selective MDM2 inhibitor undergoing phase 1 clinical trials in p53wt tumors

Philipp Holzer*, Keiichi Masuya[†], Pascal Furet, Joerg Kallen, Therese Valat-Stachyra, Stéphane Ferretti, Joerg Berghausen, Michèle Bouisset-Leonard, Nicole Buschmann, Carole Pissot-Soldermann, Caroline Rynn, Stephan Ruetz, Stefan Stutz, Patrick Chène, Sébastien Jeay, Francois Gessier

Novartis Institutes for BioMedical Research, 4002 Basel, Switzerland

ABSTRACT As a result of our efforts to discover novel p53-MDM2 protein-protein interaction inhibitors useful for treating cancer, the potent and selective MDM2 inhibitor NVP-CGM097 (**1**) with an excellent in vivo profile was selected as a clinical candidate and is currently in phase 1 clinical development. This article provides an overview of the discovery of this new clinical p53-

MDM2 inhibitor. The following aspects are addressed: mechanism of action, scientific rationale, binding mode, medicinal chemistry, pharmacokinetic and pharmacodynamic properties and in vivo pharmacology/toxicology in preclinical species.

Introduction

The p53 protein, also known as the "guardian of the human genome",[1] is a transcription factor that controls the cellular response to DNA damage or other stress stimuli through the induction of cell-cycle arrest, DNA repair, apoptosis or senescence.[2] Significant drug discovery efforts have been directed to block the protein-protein interaction between p53 and MDM2 (also known as HDM2, mouse double minute 2 homolog), which is an E3 ubiquitin ligase that targets p53 for degradation by the proteasome.[3] Mice lacking p53 develop normally but are prone to the development of a variety of tumors.[4] *TP53*, the gene encoding the p53 protein, is mutated or deleted in nearly 50% of human cancers, rendering p53 nonfunctional as a tumor suppressor.[5] Although *TP53* retains wild-type status in the remaining 50% of human cancers, its function is effectively regulated by a variety of complex mechanisms.[6] In tumor cells p53 is frequently inactivated, often via over-expression of MDM2 that binds p53 with high affinity, thereby promoting its degradation as well as masking its ability to activate transcription. Whereas p53 activation underlies the activity of many DNA-damaging chemotherapeutics in response to cellular stresses, a more attractive therapeutic strategy would be to competitively bind MDM2 and restore p53 levels to a threshold to induce apoptosis.[7]

Protein-protein interactions (PPIs) often span large surface areas (>1600 Å^2) and typically lack deep, well-defined binding pockets. When Kussie *et al.* published the first X-ray structure of the

N-terminal p53[17-125] binding domain of MDM2 and its analog from *Xenopus laevis* (71 percent identity to human MDM2) bound to a 15-residue peptide analog of p53 in 1996, first insights into the structural features and the amino acid side chains involved in the intracellular PPI were obtained.[8] The crystal structure showed that the interface relies on the steric complementarity between the MDM2 cleft and the hydrophobic face of the α-helix of p53, and revealed the particular importance of a triad of p53 amino acids. The side-chains of Phe-19, Trp-23 and Leu-26 have extended conformations and pack closely to each other, making sequential and extensive van der Waals contacts with the surface of MDM2. These observations led Novartis scientists to publish pioneering work in 2000, where the critical roles of these residues in molecular recognition were demonstrated in experiments performed with phage display peptide libraries.[9] In this work peptide-scanning investigations identified an 8-mer peptide with a key 6-chlorotryptophan residue which gave a 63-fold enhancement in activity relative to the corresponding tryptophan analog and inhibited full-length p53 binding to Glutathione S-transferases (GST) tagged MDM2 with an IC_{50} value of 5 nM. Although the initial interest of polypeptides to target p53/MDM2 was limited due to their poor membrane permeability and physiological stability, the pharmacophore model that emerged from this work propelled the identification of both peptide-like and non-peptidic inhibitors for this target.

Parallel to the p53/MDM2 PPI disruptors obtained by screening proprietary compound collections,[10] in silico approaches have also been used by several groups to assist in the search for hits for this target. Using our acquired internal knowledge, the "central valine concept" was established using molecular modeling to orient in 3D the key pharmacophores via a central connecting fragment. This led to the discovery of two new p53-MDM2 inhibitor scaffolds based on a 3-imidazolyl indole[11] and a tetrasubstituted imidazole core structure.[12] Parallel to these

efforts and seeking to extend chemical space, a large scale knowledge-based virtual screening exercise was undertaken.[13] Medicinal chemistry exploration of one of the virtual screening hits allowed us to identify dihydroisoquinolinone derivatives as an additional new class of p53-MDM2 inhibitors.[14] Optimization of this new series of inhibitors has culminated in compound **1** (NVP-CGM097), a compound currently being evaluated in phase 1 clinical trials.[15,16] Several other small molecule MDM2 antagonists have also recently progressed into clinical trials and a compilation of known chemical matter has recently been published.[17] In this paper, we provide an overview of the scientific efforts resulting in the discovery of **1**.

Development of the dihydroisoquinolinone series using X-ray structural information[14,18]

Starting from a virtual screening hit, we identified a new class of inhibitors of the p53-MDM2 interaction having an isoquinolinone core structure.[14] An initial optimization effort guided by crystal structure information afforded compound **2**, a potent MDM2 inhibitor with an IC_{50} of 8 nM in the TR-FRET biochemical assay (**Figure 1** and **Table 1**).[19] Compound **2** demonstrated significant activity in the SJSA-1 cell proliferation assay (IC_{50} of 3.86 μM) and was therefore an interesting starting point for further development. We succeeded in rapidly generating an X-ray co-crystal structure of **2** with MDM2 (**Figure 1**), which was key to guiding our optimization strategy. It confirmed the binding mode for this class of compounds and the preference of the C1 stereo center, bearing the para-chlorophenyl group, for the (S) configuration. This observation aligned well with data from the TR-FRET biochemical assay with a measured IC_{50} of 2.3 nM for the pure C1-(S)-stereoisomer **3** compared to an IC_{50} of 1.17 μM for the C1-(R)-stereoisomer **4**. The co-crystal structure showed that all three critical binding pockets (Leu-26, Trp-23, and Phe-

19) of MDM2 were occupied by compound **2**. Consistent with the previously observed SAR, the C7-(R)-sec-butoxy and the C1 p-chlorophenyl residues of **2** bind efficiently in the Leu-26 and Trp-23 binding pockets of MDM2 respectively, suggesting limited options to form additional favorable interactions with MDM2 at these positions.[14] In contrast, the analysis of the X-ray co-crystal structure suggested some opportunities to improve the interaction with the Phe-19 pocket, occupied by the 4-pyridinyl moiety of **2** which is surrounded by residues Tyr-67, Met-62 and Gln-72 of MDM2, according to the X-ray structure (**Figure 1**). The 4-pyridine ring of **2** adopts an almost parallel orientation with respect to the phenol ring of Tyr-67, consistent with the original design concept where an aromatic stacking interaction with Tyr-67 was sought.[14] Supported by molecular modeling, we then investigated other binding possibilities within the Phe-19 pocket of MDM2, in particular van der Waals contacts with Met-62 and H-bond interactions with Gln-72. The replacement of the 4-pyridinyl moiety of **2** by cyclic amines or cycloalkyl motifs substituted by amino functions, were modeled and suggested a unique opportunity to interact with both residues at the same time. The piperidine derivative **5** and the trans-cyclohexyl amine derivative **6** were the most promising analogs with a 2 – 3 fold gain of potency over **2** in both TR-FRET biochemical and SJSA-1 cellular proliferation assays. Furthermore, dialkylation of analog **6** was well tolerated and led to compounds with slightly improved potencies, as illustrated by the dimethylamine analog **7**. In addition to good potency in the SJSA-1 proliferation assay (IC_{50} of 0.94 μM), its C1-(S)-stereoisomer **8** possessed interesting in vitro ADME properties such as high solubility in our high-throughput equilibrium assay (>1 mM at pH 6.8), high permeability in our PAMPA assay ($logP_e$ of -4.4) and a intrinsically low metabolic clearance in rat liver microsomes (CL_{int} of 5.6 μl.min^{-1}.mg^{-1} and $t_{1/2}$ of 246 min). The only liabilities identified were time-dependent inhibition (TDI) of cytochrome P450 3A (k_{obs} of

0.042 min^{-1}) and inhibition of the hERG receptor (IC$_{50}$ of 1.3 μM in the hERG radioligand

binding assay).

To further characterize our benchmark compound **8**, we performed a rat pharmacokinetic (PK)

experiment (**Table 4**). Not surprisingly, compound **8** exhibited typical PK parameters for a

compound bearing a basic tertiary amine, meaning a very high volume of distribution (Vss of

23.9 L.kg^{-1}) associated with a long half-time (t$_{1/2}$ of 19.1 h). Whereas the low to medium in vivo

clearance in rat (CL of 15 ml.min^{-1}.kg^{-1}) was consistent with measured in vitro data, the

relatively low oral bioavailability was disappointing and suggested an absorption issue not

anticipated based on its in vitro solubility / permeability balance. Further characterization of the

permeability profile of **8** in the Caco-2 cell permeability assay revealed an asymmetric recovery

of the compound (A-B recovery below 30%, a Papp A-B of 0.08 (10^{-6}cm.s^{-1}) and a Papp B-A of

0.12 (10^{-6}cm.s^{-1})). As the Caco-2 cell permeability assay can predict human oral absorption and

identify passively transported compounds, these initial data suggest that the PAMPA assay had

overestimated the permeability of our compound and the Caco-2 data better explain the low oral

absorption of compound **8**. Close analogs of **8** were obtained by varying the isobutyl group

occupying the leucine pocket of MDM2. Switching to an achiral isopropoxy group notably

resulted in the identification of **9** with similar cellular potency while simplifying the structure of

our molecules by removing the stereocenter. In conclusion, the profiling of compound **8** and the

identification of **9** highlighted a certain number of challenges which directed our focus to: a)

reducing the basicity to improve permeability and cell potency and b) exploring possibilities to

reduce the lipophilicity of the compounds and at the same time potentially increasing the fu

(fraction unbound) via reduction of the plasma protein binding (PPB). The influence of

molecular properties on the likelihood of success for compounds moving into development was

initiated by Lipinski and his "Rule of Five".[21] But more recently, the attention has focused on the understanding of the physicochemical properties on in vivo toxicological outcomes.[22]

Modulating the basicity in the dihydroisoquinolinone series[18]

The replacement of the basic dimethylamine on the cyclohexyl side chain by amides, for example a compound where the 4-aminocyclohexyl is extended to propionamide (compound **10**) showed an $IC_{50} > 30$ μM in the hERG radioligand binding assay, however displayed clearly reduced potency in the biochemical TR-FRET assay with an IC_{50} of 20 nM (**Table 1**). As the basic dimethylamine appeared to be favorable for potency, we synthesized additional analogs which maintained the basic group. According to our SAR knowledge and the geometry of the Phe-19 binding pocket of MDM2, we focused our investigations on cyclic analogs, which were designed to nicely occupy the Phe-19 binding region as well as modulating the basicity of the remaining basic center. We rapidly identified very potent compounds such as the imidazolidin-4-one **11** and the piperazin-2-one **12**, see **Table 2**, both showing similar or slightly improved potency compared to **9** in the SJSA-1 proliferation assay with IC_{50}'s of 0.60 and 0.35 μM respectively. As expected, the basicity of the tertiary amine of compound **12** (calculated pKa of 8.05 ± 0.59 using MoKa[20] was significantly reduced compared to the dimethylamine analog **8** (calculated pK_a of 10.4 ± 0.59) leading to a ~ 10-fold reduction of the hERG activity (IC_{50} of 16 μM for compound **12** vs 1.3 μM for compound **8**).

The reduced basicity of the tertiary amine of compound **12** had favorable effects on its PK properties (**Table 4**). In comparison with compound **8**, compound **12** had a much lower volume of distribution (Vss of 8.0 L.kg^{-1}) and a reduced half-life ($t_{1/2}$ of 9.3 h) while its clearance

remained moderate (CL of 12 ml.min^{-1}.kg^{-1}) in rats. More importantly, the measured absorption

was quicker and more complete reaching a maximum at 4 hours and resulting in a ~ 3 fold higher

oral exposure and oral bioavailability than for **8**. The improved absorption profile of compound

12, where a bioavailability of 49% was reached, was achieved despite the permeability of

compound **12** being significantly lower than for **8** or **9** as assessed in the PAMPA assay (**Table

2**). Further N-alkylation of the piperazinone group with the aim of increasing permeability led to

the discovery of compound **1**. The additional N-methyl substituent significantly increased

permeability as assessed in our PAMPA assay (logP$_e$ of -4.6), while maintaining very good

cellular potency in the SJSA-1 proliferation assay (IC$_{50}$ of 0.35 μM) and good metabolic stability

in monkey and human liver microsomes (**Table 3**). These overall good properties of compound **1**

translated to favorable PK properties in rats (see **Table 5**) where the compound exhibited a low

clearance (CL of 7 ml.min^{-1}.kg^{-1}) and moderate volume of distribution (Vss of 6.4 L.kg^{-1}),

accompanied by a ~ 2-3 fold increase in oral exposure and bioavailability compared to **12**.

As stated earlier, while efforts were focused on reducing the overall basicity of our

compounds, we also explored in parallel possibilities to reduce lipophilicity. As we succeeded on

the first part and the basicity of our compounds was reduced significantly, the lipophilicity to

some extend increased. In our attempts to improve the overall physico-chemical properties of the

compounds, especially with regard to their solubility at neutral pH, positions in the molecules

were probed for accommodating polarity. One opportunity was to replace the central phenyl ring

with a nitrogen-containing heterocycle, such as pyridine. This idea was supported by modeling

as the introduced polarity was expected to point towards the solvent-exposed region and not to

be involved in any key interactions. A series of derivatives was synthesized and the results are

summarized in **Table 3**. Through the introduction of the nitrogen in the phenyl ring, the

measured logP could be reduced by at least one log unit. Thus, **1** has a measured logP of 5.8 whereas compounds **15** and **16** have logP values of 4.8 and 4.6, respectively. In parallel, the calculated polar surface area increases from 65.6 Å^2 for **1** up to 91.3 Å^2 for compound **17**. While most of the compounds retained their biochemical potency, confirming the tolerance of polarity in this binding region, they clearly showed reduced liver microsomal stabilities in human and monkey species, compared to **1**.

Compound 1 binding to MDM2 is species dependent

It was interesting to observe that the dihydroisoquinolinone series demonstrated species specific effects with respect to MDM2 binding. A comparison of the potency of compound **1** and Nutlin-3a[10] on MDM2 from different species (human, dog, mouse and rat proteins) (**Figure 2A**) revealed only minimal deviations between species for Nutlin-3a whereas significant variation was observed with **1**. This compound is 16-fold more potent on human than dog MDM2 and 51- and 37-fold more potent on human than mouse and rat MDM2, respectively.

A careful analysis of the peptide sequence of MDM2 in the p53 binding pocket identified two amino acid differences: Leu-54 and Leu-57 in the human sequence are switched to isoleucines in rodent species, see **Figure 2B**. The additional methyl groups in Ile-54 and -57 result in slightly larger side chains which protrude into the binding pocket. This leads to a steric clash (see **Figure 2C**) resulting in a weaker binding affinity and a loss in potency in rodents. In dog, one of the leucins (Leu54) is replaced by isoleucin which results in a 16-fold reduced binding affinity. As the monkey to human sequences are the same, we concluded that the required toxicity studies to assess the on-target toxicity would need to be evaluated in non-human primate (NHP). As a

consequence, the measured monkey liver microsomal stability became very important as well as

the monkey in vivo PK. Comparing the monkey liver microsomal stability of compounds **1** and

14, the low in vitro clearance of **1** translated well into the in vivo situation (CL 4 ml.min^{-1}.kg^{-1}).

Pharmacokinetic profiles of compound 1 in preclinical species

The non-compartmental PK parameters of **1** estimated in blood of OF-1 mouse, Sprague-

Dawley rat, Beagle dog and Cynomolgus monkey after a single oral (p.o.) or intravenous (i.v.)

dose are shown in **Table 5**. After i.v. administration, the total blood clearance (CL) of **1** was 5

ml.min^{-1}.kg^{-1} for mouse, 7 ml.min^{-1}.kg^{-1} for rat, 3 ml.min^{-1}.kg^{-1} for dog and 4 ml.min^{-1}.kg^{-1} for

monkey. Based on the respective hepatic blood flows, **1** showed a consistent low total blood CL

in all species (5 to 10% of hepatic blood flow). The estimated volume of distribution at steady-

state (Vss) was in the range of 2 to 6 L.kg^{-1} in all species indicating moderate tissue distribution.

The apparent terminal half-life ($t_{1/2}$) was long in rodents and monkey (6 to 12 h), but was

comparatively longer in dogs (20 h). After oral dosing, the compound was well absorbed with

T_{max} occurring between 1 and 4.5 h in all species tested. The oral bioavailability (%F) was high

in mouse, rat and dog, and moderate in monkey.

With its combination of high potency and excellent physicochemical and pharmacokinetic

properties, compound **1** was selected for further development towards a clinical candidate.

Binding mode – X-ray of 1 bound to MDM2

As illustrated in **Figure 3**, The dihydroisoquinolinone scaffold of compound **1** occupies the

middle of the binding site and provides the appropriate exit vectors to reach the three critical

binding pockets of the p53 residues Leu-26, Trp-23, and Phe-19. The isopropyl ether at C7 and

the methyl ether at C6 fill the Leu-26 pocket and the ether oxygens make water-mediated H-

bond interactions with the OH of Tyr-100 and the carbonyl of Gln-24, while the C1 4-

chlorophenyl group reaches deep into the Trp-23 binding cavity. The C3 carbonyl function of the

dihydroisoquinolinone scaffold is engaged in a water-mediated H-bond interaction with the

carbonyl oxygen of Phe-55 and therefore contributes to the overall affinity of the molecule. More

importantly, it induces a conformational constraint to the N-aryl side-chain next to it, providing

the right torsion angle to ideally enter the Phe-19 binding region. The front of the pocket is

closed as Phe-55 swings up and displays a face-to-edge interaction with the

dihydroisoquinolinone core. The movement of Phe-55 is specific to this scaffold. The dialkylated

aniline functionality affords the proper exit vector and projects the methyl residue deep into a

small hydrophobic cavity on one side, and the trans-cyclohexyl moiety on the other side to nicely

occupy the central part of the Phe-19 binding region. Finally, the N-methyl piperazinone motif

binds towards the exit of the Phe-19(p53) binding cavity in a water-rich region and nestles

perfectly between the protein walls, contributing significantly to the potency of **1**.

Chemical synthesis of compound 1

Compound **1** and related analogs described in this paper were synthesized according to the

convergent route presented in **Scheme 1**. The asymmetric synthesis of the key (S)-

isoquinolinone intermediate **23** was accomplished in 5 linear steps starting with the alkylation of

the commercially available (4-hydroxy-3-methoxy-phenyl)-acetic acid ethyl ester. Intermediate

18 was selectively formylated para to the methoxy group with dichloro(methoxy)methane to give

the aldehyde **19** in good yield. Condensation of the aldehyde functionality with the (S)-2-

methylpropane-2-sulfinamide following the published reaction conditions from Davis *et al.*[23]

delivered the enantiopure (S)-sulfinylimine **20**, which was used as a chiral auxiliary for the

enantioselective introduction of the p-chlorophenyl moiety. Classical nucleophiles such as

Grignard or organolithium derivatives reacted much faster on the ethyl ester of **20** leading to the

formation of side-products only. Following a methodology developed by Inoue *et al.*,[24] the

desired sulfinylamine **22** was finally obtained with a diastereoselectivity of 96:4 by the addition

of the arylstannane **21** to the (S)-sulfinylimine **20** using the rhodium complex

$[Rh(cod)(MeCN)_2]BF_4$ as a catalyst. Acidic cleavage of the sulfoxamine group generated the

corresponding primary amine which reacted with the neighboring ester under basic conditions to

deliver the key isoquinolinone intermediate **23** in nearly quantitative yield and with an

enantiomeric excess of 92%. The preparation of the isoquinolinone **23** as a pure (S)-stereoisomer

constituted an important boost for the preparation of the whole series by avoiding the time

consuming chiral separation of all final compounds of interest.

The side chain of **1** was synthesized in six linear steps following the sequence shown in

Scheme 1. Reductive amination of the commercially available (4-formyl-cyclohexyl)-carbamic

acid tert-butyl ester with 4-iodoaniline using $NaBH(OAc)_3$ as a reductant led to the intermediate

24. The same reaction conditions were employed in the subsequent step but using formaldehyde

to produce the N-methyl analog **25**. Acidic cleavage of the Boc-protecting group led to the free

amine **26**, which was selectively mono-alkylated with methyl 2-bromoacetate at low temperature

to give the amino ester **27**. The remaining free position on the amino functionality was further

alkylated with methyl-(2-oxo-ethyl)-carbamic acid tert-butyl ester using similar reductive

amination conditions as described above to give the intermediate **28**. Acidic cleavage of the Boc-

protecting group of **28** led to the corresponding N-methyl amine which cyclized with the

neighboring ester under basic conditions to deliver the iodo analog **29** in good yields. Finally,

both components **23** and **29** were combined under cross-coupling reaction conditions developed

by Buchwald *et al.*,[25] using copper(I) iodide as a catalyst and (+/-)-trans-1,2-diaminocyclohexane

as a ligand, to provide **1** with greater than 98% chemical purity and an enantiomeric excess of

92%. In the process of further characterization of compound **1**, a bisulfate salt has been

identified. Recrystallization allowed compound **1** to be isolated with improved enantiomeric

purity with ee >99%. In addition, the crystalline form provides improvements in solubility and

stability compared to the free base amorphous form.

Profile and potency of 1, selectivity among other PPI

The binding of compound **1** was characterized by several biochemical and biophysical

methods. The data for **1** is provided in **Table 6A** and compared to Nutlin-3a. Compound **1** binds

to human MDM2 with an IC_{50} of 1.7 nM and shows high selectivity over MDM4 (IC_{50} = 2000

nM). Compound **1** is about 4-times more potent than Nutlin-3a (IC_{50} = 8.0 nM).

To understand the thermodynamic parameters of the interactions in solution, isothermal

titration calorimetry (ITC) was carried out using **1** and human MDM2 (using the construct

MDM2[14-111;L33E]). The thermodynamic signature is shown in **Table 6B**. Overall, both the

ΔH and $-T\Delta S$ contributions are favorable (i.e. negative), which correlates with the favorable van

der Waals interactions made by compound **1** which do not lead to a strong rigidification of

MDM2. Finally, as shown in **Table 6C**, a thermal shift assay, also called Differential Scanning

Fluorimetry (DSF), was done to measure the thermal stability increase of human MDM2 upon

binding of **1** to the protein. For compound **1**, thermal stabilization with a ΔT of 25°C was

observed, which correlates with the low nM affinity.

Compound **1** selectivity was evaluated in a number of biochemical assays to assess its activity

against multiple binding partners, including the p53:MDM4 interaction (MDM4 protein being

closely related to MDM2). In TR-FRET assays, as described in **Table 6D**, compound **1** was

shown to be selective for the p53:MDM2 interaction compared to the p53:MDM4 interaction

(1'176-fold selectivity) and the Ras-Raf interaction (3'000-fold selectivity). In addition, **1**

showed no significant activity against Bcl-2:Bak, Bcl-2:Bad, Mcl-1:Bak, Mcl-1:NOXA,

XIAP:BIR3 and c-IAP:BIR3 protein-protein interactions.

Activity of compound 1 in cell-based models

Potency of p53:MDM2 interaction inhibitors can be evaluated in cells with wild-type p53.

Disruption of the p53:MDM2 interaction should release p53 from MDM2, leading not only to a

stabilization but also to a nuclear translocation of p53. Compound **1**-induced p53 nuclear

translocation can be evaluated in p53 wild-type cells using a mechanistic p53 re-distribution

assay (based on the GRIP® technology) and can be quantified with a high-content imaging

platform. As shown in **Table 7**, compound **1** was able to significantly re-distribute wild-type p53

into the cell nucleus with an IC_{50} of 0.224 μM, demonstrating its ability to inhibit the

p53:MDM2 interaction in living cells. In addition, compound **1** activity against the p53:MDM2

interaction was assessed in proliferation assays using either wild-type p53 or p53 null cells. Two

pairs of cell lines were used to assess compound **1** p53-dependent anti-proliferative effects: 1) an

isogenic pair of HCT116 cell lines either expressing wild-type p53 or knocked-out for the p53

gene and 2) a non-isogenic pair of osteosarcoma cell lines either endogenously expressing wild-

type p53 and amplified for MDM2 (SJSA-1 cells) or null for p53 (SAOS-2 cells). As indicated in

Table 7, compound **1** significantly inhibited the proliferation of cells expressing wild-type p53,

while sparing the p53 null cells with a 35 to 58-fold difference. Overall, these results indicate

that **1** inhibits the p53:MDM2 interaction in cells, leading to p53 nuclear translocation that

results in cell growth inhibition, in a p53-dependent manner.

In vivo anti-tumor activity of compound 1

Compound **1** was able to inhibit the interaction between p53 and MDM2 and reactivate the p53

pathway in vivo in a MDM2- amplified SJSA-1 human tumor model, as judged by elevation of

p21 mRNA levels, a pharmacodynamic (PD) indicator for p53 activity.[26] As shown in **Figure 5**,

p21 mRNA levels were found to increase concomitantly with levels of compound **1** in tumor-

bearing rats dosed at 30 mg/kg. The PD response was bi-phasic and prolonged up to 24 h.

Additional p53 target genes such as MDM2 and PUMA mRNA levels were assessed in the

tumor samples as well and showed a similar behavior.

Daily treatment with **1** dose-dependently and significantly inhibited SJSA-1 tumor growth in

rats (**Figure 6**). It promoted stable disease at 20 mg/kg which was associated with a plasma

AUC_{0-24} of 163 µM.h (**Table 8**). The treatment dose at 30 mg/kg, dosed daily, induced >85%

tumor regression. The 3qw (treatment on Monday, Wednesday, and Friday) treatment dose-

dependently and significantly affected SJSA-1 tumor growth. It induced a T/C of 25% at 30

mg/kg and full tumor regression at 70 mg/kg which was associated with a plasma AUC_{0-24} of 616 $\mu M.h$ and a plasma AUC_{0-48} of 1045 $\mu M.h$ (**Table 8**). 3qw treatment was well tolerated at all the doses and no histopathology findings related to the compound were made. For the daily treatment, histopathology was performed for the 30 mg/kg dose and no histopathology findings related to the compound were made either. The fact that the doses were well tolerated was not a surprise to us, considering the human MDM2 specificity of **1**, as described above. In summary, **1** shows dose-proportional increases in exposure and a clear PK/PD relationship, resulting in tumor growth inhibition effects at well-tolerated doses in tumor-bearing rats. Dosing schedules have been investigated and indicate that **1** inhibits tumor growth in rats, not only on a daily dosing schedule but also when animals are treated 3-times a week.

Compound 1 in toxicity studies

Following repeated-dose oral administration, the bone marrow, the lymphoid organs, the GI tract and the testes (organs with a high degree of cell turnover) were identified as target organs of toxicity in the monkey. In the rat, compound **1**-related microscopic findings were present in the testes, heart (males only) and adrenal gland (both gender). It should be noticed that in rats, the lesion in the testes was a subtle structural change affecting the tubular epithelium (no effect on proliferative cells), in contrast to the monkey where germinal cells were affected. Thus, actively dividing cells in the rat testes were not affected in contrast to the monkey testes.

The changes observed in the 4-week GLP studies were consistent with the non-GLP 2-week DRF studies and were treatment duration- and dose-dependent. All changes showed complete or partial reversibility after 4 weeks. Based on the similar potency of compound **1** against the

p53/MDM2 protein-protein interaction in humans and Cynomolgus monkey, the latter is

considered a good predictor of pharmacological and toxicological responses in humans. In

contrast, the potency towards p53/MDM2 protein-protein interaction is 63-fold lower in rat than

in human. Although monkeys are expected to more accurately predict human pharmacological

response to **1** and any resulting on-target toxicity, the rat may also predict off-target effects not

observed in monkeys.

Conclusion

A combination of a good understanding of the target and its binding pocket, virtual screening,

X-ray crystallography, molecular modeling and iterative medicinal chemistry resulted in the

discovery of the dihydroisoquinolinone series. Within this novel series, compound **1** was

identified as a potent and selective human MDM2 inhibitor with excellent in vitro and in vivo

characteristics. Compound **1** is currently undergoing phase 1 clinical trials in p53wt tumors.

AUTHOR INFORMATION

Corresponding Author

* P.H.: (phone, office) +41 61 696 2087; (email) philipp.holzer@novartis.com

Present Addresses

† PeptiDream Inc., 4-6-1 Komaba, Meguro-ku, Tokyo, 153-8904, Japan

Notes

ABBREVIATIONS

3qw, three times per week dosing; AcOH, acetic acid; AUC, area under the curve; CL, clearance; CMC, carboxymethyl cellulose ; CYP, cytochrome P450; DCM, dichloromethane; DMF, N,N-diemethylformamide; DMSO, dimethylsulfoxide; dr, diastereoselectivity ratio; DSF, differential scanning fluorimetry; ee, enantiomeric excess; er, enantioselectivity ratio; EtOAc, ethyl acetate; EtOH, ethanol; GI_{50}, concentration causing 50% growth inhibition; aq. HCHO, aqueous formaldehyde; HDM2, human analog of MDM2; HPMC, hydroxypropyl methyl cellulose; fu, fraction unbound; HTS, high-throughput screening; IC_{50}, half maximal inhibitory concentration; ITC, isothermal titration calorimetry; iv, intravenous; K_2CO_3, potassium carbonate; LM, liver microsome; MeOH, methanol; MDM2, murine double minute 2; NHP, non-human primate; NMR, nuclear magnetic resonance; PD, pharmacodynamic; PK, pharmacokinetics; PSA, polar surface area; q24h, once a day dosing; qRT-PCR, reverse transcription polymerase chain reaction; RT, room temperature; SAR, structure − activity relationship; SD, standard deviation;

SEM, standard error of mean; TDI, time dependent inhibition; TFA, trifluoroacetic acid; THF, tetrahydrofuran; TLC, thin layer chromatography; TR-FRET, time resolved fluorescence resonance energy transfer; V_{SS}, volume of distribution.

Supporting Information Available: Synthesis procedures of compound **1** has been provided. This material is available free of charge via the Internet at http://pubs.acs.org.

REFERENCES

1. Lane, D.P.; p53, Guardian of the genom. *Nature* **1992**, *358*, 15–16.

2. Harris, S. L.; Levine, A. J.; The p53 pathway: positive and negative feedback loops. *Oncogene* **2005**, *24*, 2899-2908.

3. Michael, D.; Oren, M.; The p53-Mdm2 module and the ubiquitin system. *Semin. Cancer Biol.* **2003**, *13*, 49-58.

4. Kemp, C. J.; Donehower, L. A.; Bradley, A.; Balmain, A.; Reduction of p53 gene dosage does not increase initiation or promotion but enhances malignant progression of chemically induced skin tumors. *Cell* **1993**, *74*, 813−822.

5. Feki, A.; Irminger-Finger, I.; Mutational spectrum of mutations in primary breast and ovarian tumors. *Crit. Rev. Oncol. Hematol.* **2004**, *52*, 103−116.

6. Kruse, J.-P.; Gu, W.; Modes of p53 regulation. *Cell* **2009**, *137*, 609-622.

7. Khoo, K. H.; Verma, C. S.; Lane, D. P.: Drugging the p53 pathway: understanding the route to clinical efficacy. *Nature Rev. Drug Discov.* **2014**, *13*, 217-236.

8. Kussie, P. H.; Gorina, S.; Marechal, V.; Elenbaas, B.; Moreau, J.; Levine, A. J.; Pavletich, N. P.; Structure of the MDM2 oncoprotein bound to the p53 tumor supressor transactivation domain. *Science* **1996**, 274, 948-953.

9. García-Echeverría, C.; Chène, P.; Blommers, M.; Furet, P.; Discovery of potent antagonists of the interaction between human double minute 2 and tumor suppressor p53. *J. Med. Chem.* **2000**, *43*, 3205-3208.

10. Vassilev, L. T.; Vu, B. T.; Graves, B.; Carvajal, D.; Podlaski, F.; Filipovic, Z.; Kong, N.; Kammlott, U.; Lukacs, C.; Klein, C.; Fotouhi, N.; Liu, E. A.; In vivo activation of the p53 pathway by small-molecule antagonists of MDM2. *Science* **2004**, *303*, 844-848.

11. Furet, P.; Chene, P.; De Pover, A.; Valat, T.; Hergovich Lisztwan, J.; Kallen, J.; Masuya, K.; The central valine concept provides an entry in a new class of non peptide inhibitors of the p53-MDM2 interaction. *Bioorg. Med. Chem. Lett.* **2012**, *22*, 3498-3502.

12. Vaupel, A.; Bold, G.; De Pover, A.; Stachyra-Valat, T.; Hergovich Lisztwan, J.; Kallen, J.; Masuya, K.; Furet, P.; Tetra-substituted imidazoles as a new class of inhibitors of the p53-MDM2 interaction. *Bioorg. Med. Chem. Lett*. **2014**, *24*, 2110–2114.

13. Jacoby. E.; Boettcher, A.; Mayr, L.; Brown, N.; Jenkins, J.; Kallen, J.; Engeloch, C.; Schopfer, U.; Furet, P.; Masuya, K.; Knowledge-based virtual screening: application to the MDM4/p53 protein-protein interaction. *Methods Mol. Biol.* **2009**, *575*, 173-194.

14. Gessier, F.; Kallen, J.; Jacoby, E.; Chène, P.; Stachyra-Valat, T.; Ruetz, S.; Jeay, S.; Holzer, P.; Masuya, K.; Furet, P.; Discovery of dihydroisoquinolinone derivatives as novel inhibitors of the p53-MDM2 interaction with a distinct binding mode. *Bioorg. Med. Chem. Lett.*, **2015**, DOI: http://dx.doi.org/10.1016/j.bmcl.2015.06.058.

15. Jeay, S.; Gaulis, S.; Ferretti, S.; Bitter, H.; Ito, M.; Valat, T.; Murakami, M.; Ruetz, S.; Guthy, D.A.; Rynn, C.; Jensen, M. R.; Wiesmann, M.; Kallen, J.; Furet, P.; Gessier, F.; Holzer, P.; Masuya, K.; Würthner, J.; Halilovic, E.; Hofmann, F.; Sellers, W. R.; Graus Porta, D.; A distinct p53 target gene set predicts for response to the selective p53-HDM2 inhibitor NVP-CGM097. eLife **2015**; DOI: 10.7554/eLife.06498.

16. Collingwood, S.P.; Ratcliffe, A.J.; Pryde, D.; Porter, R.; Recent disclosures of clinical candidates: highlights from the Society for Medicines Research symposium, held December 4, 2014 – National Heart & Lung Institute, London, UK. *Drug Future*, **2015**, *40*, 81-91.

17. Neochoritis, C.; Estrada-Ortiz, N.; Khoury, K.; Dömling, A.; p53–MDM2 and MDMX antagonists. *Annu. Rep. Med. Chem.*, **2014**, *49*, 167-187.

18. Berghausen, J.; Buschmann, N.; Furet, P.; Gessier, F.; Hergovich Lisztwan, J.; Holzer, P.; Jacoby, E.; Kallen, J.; Masuya, K.; Pissot-Soldermann, C.; Ren, H.; Stutz, S.; Substituted isoquinolinones and quinazolinones; WO 2011076786 A1.

19. Routinely, inhibitory effects of our compounds on p53-MDM2 or p53-MDM4 binding were measured by a Time-Resolved Fluorescence Resonance Energy Transfer (TR-FRET) assay and expressed as the concentration causing 50% inhibition (IC_{50}). Compounds at different concentrations were added to 0.1 nM Europium-labeled streptavidin (Perkin Elmer), 0.1 nM

biotinylated MDM2 or MDM4 p53 binding domain and 10 nM Cy5-p53 aa18-26 (unpublished results).

20. Milletti, F.; Storchi, L.; Sforna, G.; Cruciani, G.; New and original pKa prediction method using grid molecular interaction fields. *J. Chem. Inf. Model*., **2007**, *47*, 2172–2181.

21. Lipinski, C.A.; Lombardo, F.; Dominy, B.W.; Feeney, P.J.; Experimental and computational approaches to estimate solubility and permeability in drug discovery and development settings. *Adv Drug Deliv Rev.*, **1997**, *23*, 3-25.

22. Hughes, J.D.; Blagg, J.; Price, D.A.; Bailey, S.; Decrescenzo, G.A.; Devraj, R.V.; Ellsworth, E.; Fobian, Y.M.; Gibbs, M.E.; Gilles, R.W.; Greene, N.; Huang, E.; Krieger-Burke, T.; Loesel, J.; Wager, T.; Whiteley, L.; Zhang, Y.; Physiochemical drug properties associated with in vivo toxicological outcomes. *Bioorg. Med. Chem. Lett*., **2008**, *18*, 4872-4875.

23. Davis, F. A.; Mohanty, P. K.; Asymmetric synthesis of the protoberberine alkaloid (S)-(-)-xylopinine using enantiopure sulfinimines. *J. Org. Chem*., **2002**, *67*, 1290-1296.

24. Oi, S.; Moro, M.; Fukurhara, H.; Kawanishi, T.; Inoue; Y.; Rhodium-catalyzed addition of arylstannanes to carbon-heteroatom double bond. *Tetrahedron*, **2003**, *59*, 4351-4361.

25. Klapars, A.; Huang, X.; Buchwald, S. L.; A general and efficient copper catalyst for the amidation of aryl halides. *J. Am. Chem. Soc*., **2002**, *124*, 7421-7428.

26. el-Deiry, W. S.; Tokino, T.; Velculescu V.E.; Levy, D. B.; Parsons, R.; Trent, J. M.; Lin, D.; Mercer, W. E.; Kinzler, K. W.; Vogelstein, B.; WAF1, a potential mediator of p53 tumor supression. *Cell*, **1993**, *75*, 817-825.

Figure 1. X-ray cocrystal structure of compound **2** bound to human MDM2 at 1.67 Å resolution (PDB code 4ZYI). MDM2 binding pockets are labeled in yellow font by p53 side chain. The stick representation is used for the MDM2 residues proximal to the 4-pyridine ring of **2**. Water molecules are not represented.
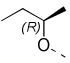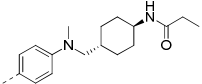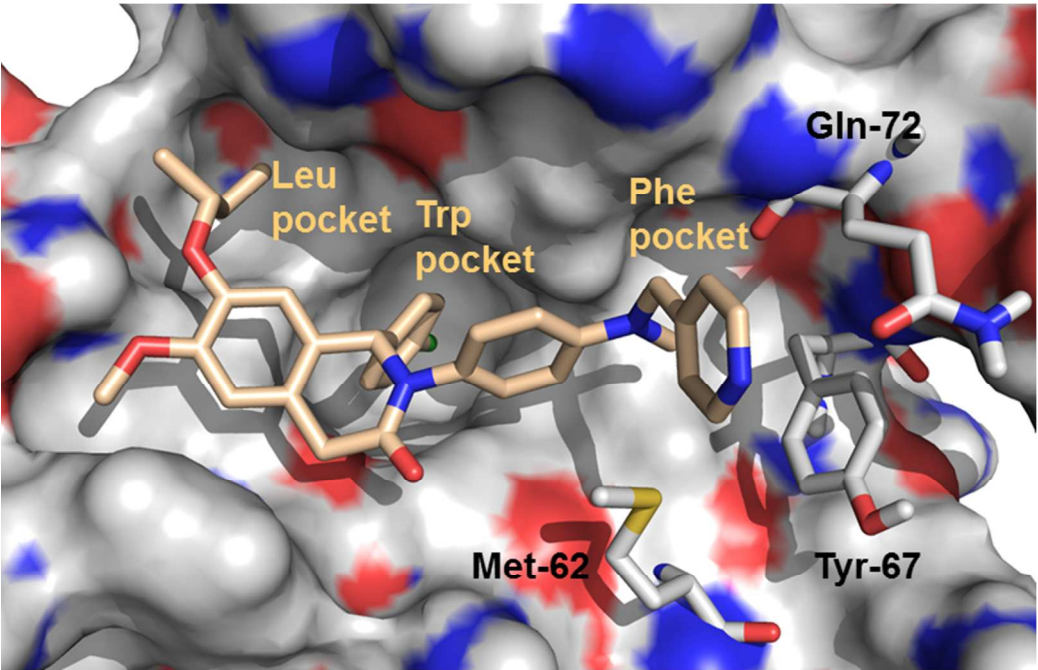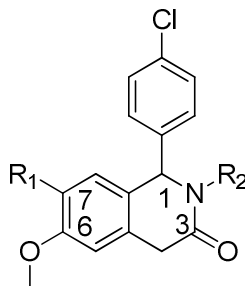
Table 1. Early SAR showing the activities of compounds **2** to **10** in the TR-FRET biochemical

assay and in the SJSA-1 cell proliferation assay.

Compound	C1-chirality	R^1	R^2	TR-FRET assay IC$_{50}$ (μM)[a] with SD	SJSA-1 cell proliferation GI$_{50}$ (μM)
2	(R/S)			0.008 [b]	3.86 [b]
3	(S)			0.0023 ±0.0004	1.21 ± 0.27
4	(R)			1.171 ±0.338	29.58 [b]
5	(R/S)			0.004 [b]	1.09 [b]
6	(R/S)			0.003 ±0.001	2.85 ± 1.69
7	(R/S)			0.003 [b]	1.13 ± 0.25
8	(S)			0.0019 ±0.0001	0.94 ± 0.015
9	(S)			0.0011 ±0.0002	0.71 ± 0.23

| 10 | (S) | | | 0.020 ±0.002 | 4.96 ± 3.45 |

[a] Values are expressed as the mean ± standard deviation of at least three independent experiments. [b] Data provided from single experiment.

Table 2. Summary of compounds **1** and **9-12** with modified basicity on the side chain.
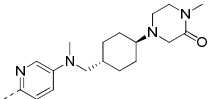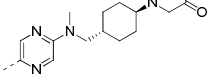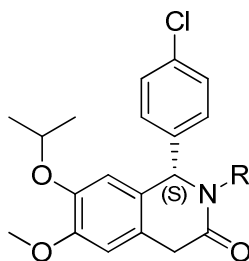

Compound	Side chain R	TR-FRET assay IC_{50} $(\mu M)^a$	SJSA-1 cell proliferation GI_{50} $(\mu M)^a$	passive permeability $logP_e$ $[10^{-6}$ cm.s$^{-1}]$
9		0.0011 ±0.0002	0.71 ± 0.23	-4.4
11		0.0017 ±0.0003	0.60 ± 0.036	-5.5
12		0.0016 ±0.0002	0.35 ± 0.17	-5.2
1		0.0017 ±0.0001	0.35 ± 0.19	-4.6

^{a} Values are expressed as the mean ± standard deviation of at least three independent experiments.

1
2
3
4
5
6
7
8
9
10
11
12
13
14
15
16
17

Table 3. Summary of selected ADME properties of dihydroisoquinolinone analogs.
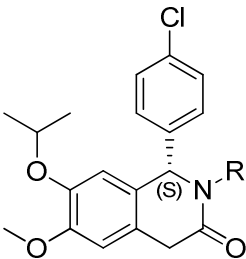
Compound	Side chain R	TR-FRET assay IC_{50} $(\mu M)^a$	CYP3A4 inhibition in human LM IC_{50} (μM)	Octanol/ Water Partition Coefficient logP	passive permeability $logP_e$ [10^{-6} cm. s^{-1}]	metabolic stability in **monkey** LM^b: CL_{int} ($\mu L.min^{-1}.mg^{-1}$)	metabolic stability in **human** LM^b: CL_{int} ($\mu L.min^{-1}.mg^{-1}$)
1		0.0017 ±0.0001	17.0	5.8	-4.6	26.6	52.3
9		0.0011 ±0.0002	9.4	>4.2^c	-4.4	n.d.	4.6
12		0.0016 ±0.0002	11.3	5.3	-5.2	79.7	3.4
13		0.0114^d	5.0	>6.3^c	n.d.	n.d.	78.3
14		0.0025 ±0.0012	13.2	4.4	-4.6	224.1	156.7
15		0.0020 ±0.0005	>20	4.8	-4.7	278.6	150.8

55
56
57
58
59
60

16		0.0076 ±0.0008	>20	4.6	-4.5	355.4	155.7
17		0.0041 ±0.0007	>20	4.6	-4.3	420	220

[a] Values are expressed as the mean ± standard deviation of at least three independent experiments. [b] LM = liver microsomes. [c] logP data point could not be determined accurately. [d] Data provided from single experiment.

Table 4. Intravenous (i.v.) and oral (p.o.) pharmacokinetic profiles of compounds **8** and **12** in rats[a].

Compound	CL (ml.min^{-1}.kg^{-1})	$t_{1/2term}$ (h)	Vss (L.kg^{-1})	AUC (i.v.) (nmol.h.L^{-1})	AUC (p.o.) (nmol.h.L^{-1})	C_{max} (nmol.L^{-1})	t_{max} (h)	%F	PPB (rat %)[b]
8	15.0 ± 1.0	19.1 ± 3.1	23.9 ± 3.0	1574 ± 128	297 ± 116	17.6 ± 5.0	7.0 ± 1.2	18 ± 5.0	>99
12	12.0 ± 1.0	9.3 ± 1.9	8.0 ± 1.8	2154 ± 207	1018 ± 346	74.6 ± 22.7	4.0 ± 1.4	49.0 ± 15.0	>99

a) dose: 1 mg/kg i.v. as a solution in NMP:PEG200 (10:90) and 3 mg/kg p.o. as a suspension in CMC:Water:Tween (0.5:99:0.5). AUC and Cmax data are dose normalized to 1 mg.kg^{-1} and data are expressed as the mean ± standard deviation from four rats. b) plasma protein binding measured by rapid equilibrium dialysis (RED) assay using 100% plasma.

Figure 2. A: Measured Ki's for comparison of the potency of compound **1** and Nutlin-3a was evaluated on MDM2 from different species (human, dog, mouse and rat proteins). **B**: Comparison of the protein sequence in the p53 binding pocket of MDM2 identified two differences in the amino acid sequence. **C**: Interactions of **1** with amino acids 54 and 57 of MDM2 results in a steric clash and reduced affinity to the binding pocket.

A

	$K_i \pm SD$ in nM (K_i ratio *vs* human)	
	1	Nutlin-3a
Human MDM2	1.3 ± 0.1 (1)	6.4 ± 1.3 (1)
Dog MDM2	20.5 ± 1.7 (16)	10.5 ± 2.0 (2)
Mouse MDM2	65.9 ± 1.0 (51)	19.9 ± 1.4 (3)
Rat MDM2	47.4 ± 10.4 (37)	12.6 ± 0.7 (2)

K_i, calculated from the TR-FRET IC_{50} using the Cheng-Prusoff equation

B Protein sequence (binding pocket)

C Interaction of NVP-CGM097 and amino acids in position 54 and 57 of MDM2 p53 binding pocket.

human and monkey MDM2   mouse and rat MDM2

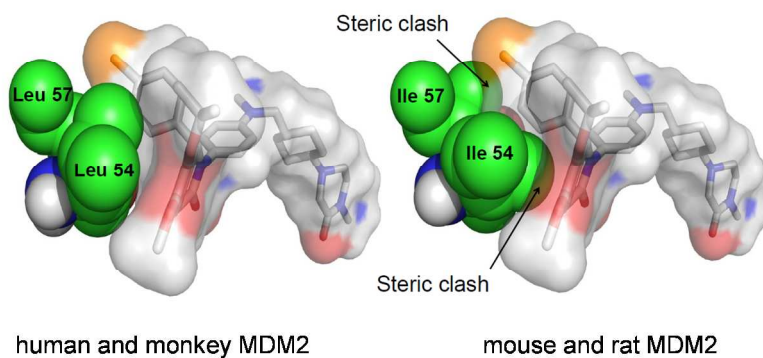**Table 5**. Summary of the calculated pharmacokinetic parameters of **1** in preclinical species [a].

PK parameter	Mouse	Rat	Dog	Monkey
Dose [i.v. ¦ p.o.] (mg/kg)	1 ¦ 3	1 ¦ 3	0.1 ¦ 0.3	0.1 ¦ 0.3
CL $(ml.min^{-1}.kg^{-1})$	5	7 ± 1	3 ± 0	4 ± 0
V_{SS} $(L.kg^{-1})$	2.6	6.4 ± 0.4	4.2 ± 0.4	2.0 ± 0.4
$t_{1/2term}$ (h)	6.4	12.1 ± 1.1	19.8 ± 2.0	8.3 ± 0.9
AUC $(nmol.h.L^{-1})$ p.o.	3337	2779 ± 385	5993 ± 797	3730 ± 777
C_{max} $(nmol.L^{-1})$ p.o.	207	134 ± 16	251 ± 30	363 ± 20
T_{max} p.o. (h)	4.0	4.5 ± 1.9	2.7 ± 1.2	1.3 ± 0.6
BAV (%F)	71	81 ± 11	74 ± 10	57 ± 12
PPB (%) [b]	>99	>99	>99	>99

a) i.v. dose provided as a solution in NMP:plasma (10:90) (mouse); NMP:PEG200 (30:70) (rat); NMP:PEG200 (10:90) (dog and monkey). p.o. dose provided as a suspension in Tween80:CMC05 (0.5:99.5) (mouse and monkey); CMC:Water:Tween (0.5:99:0.5) (rat and dog). AUC and Cmax data are dose normalized to 1 mg.kg^{-1}. Rat, dog and monkey PK data are expressed as the mean ± standard deviation from a minimum of three animals per study. In the mouse study, 3 animals were sacrificed at each timepoint over the timecourse, hence a standard deviation on reported PK values could not be calculated. b) plasma protein binding measured by rapid equilibrium dialysis (RED) assay using 100% plasma.

Figure 3. X-ray cocrystal structure of compound **1** bound to human MDM2 at 1.80 Å resolution

(PDB code 4ZYF). MDM2 binding pockets are labeled in yellow font based on the p53 side

chains which interact in these regions. The MDM2 residues that form water mediated hydrogen

bonds with **1** are shown in a stick representation as well as the mediating water molecules. Based

on the positions of the water molecule oxygen atoms observed in the X-ray structure, the water

hydrogen atoms were modelled to give consistent hydrogen bonds.
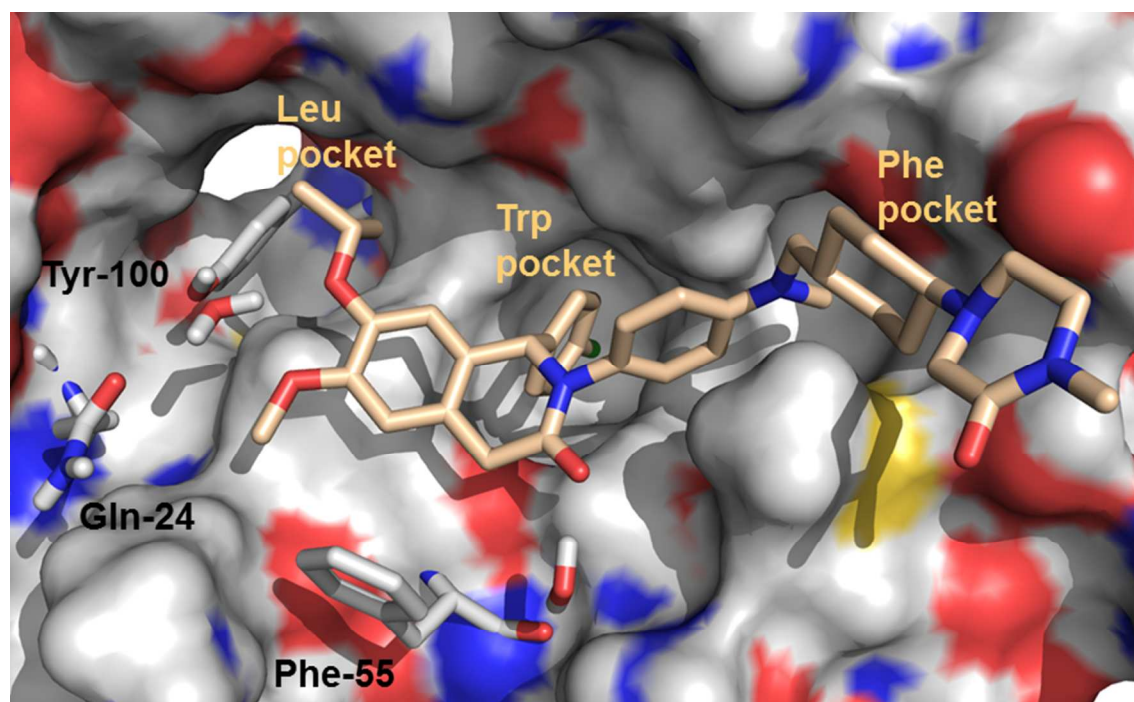
Scheme 1. Asymmetric synthesis of compound **1**.
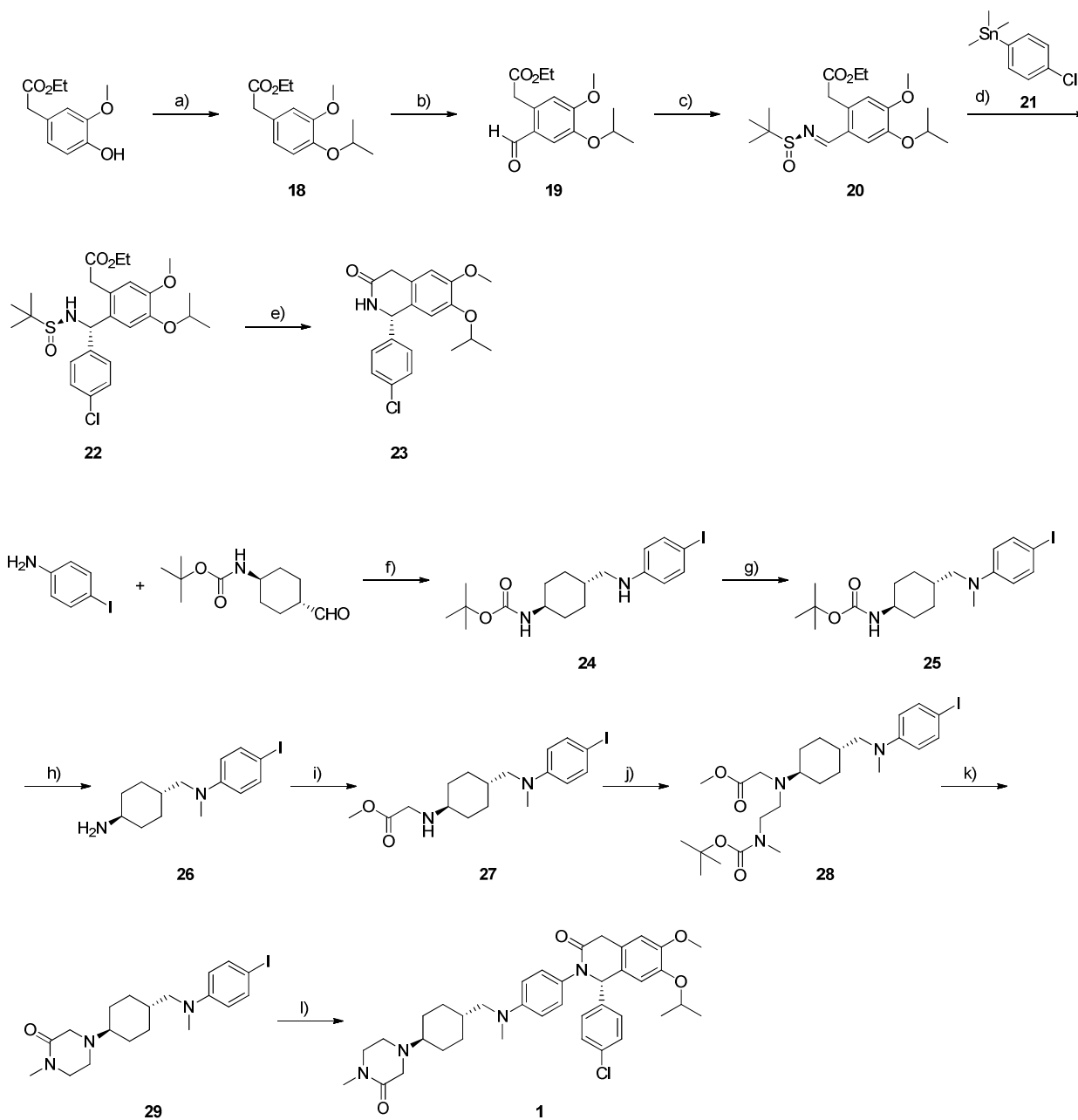
Reagents and conditions: (a) 2-iodopropane, K_2CO_3, DMF, 60°C, 5h, 89%; (b) MeOCHCl$_2$, SnCl$_4$, DCM, 0°C, 45 min, 84%; (c) (S)-(-)-2-methyl-2-propanesulfinamide, Ti(OEt)$_4$, DCM, reflux, 5h, 89%; (d) [Rh(cod)(MeCN)$_2$]BF$_4$, THF, 60°C, 6h, 28%; (e) HCl, MeOH, RT, 30 min then Et$_3$N, RT, 15 min, 91%; (f) AcOH, NaBH(OAc)$_3$, DCM, RT, 1h, 79%; (g) AcOH, aq. HCHO, NaBH(OAc)$_3$, DCM, RT, 2h, 76%; (h) TFA, DCM, RT, 30 min, 97%; (i) 2-

bromoacetate, K_2CO_3, DMF, -10°C to 10°C, 4.5h, 44%; (j) methyl-(2-oxo-ethyl)-carbamic acid tert-butyl ester, AcOH, NaBH(OAc)$_3$, DCM, rt, 1h, 97%; (k) HCl, dioxane, RT, 30 min then Et$_3$N, MeOH, RT, 1h, 86%; (l) **23**, K_3PO_4, CuI, (+/-)-trans-1,2-diaminocyclohexane, dioxane, 95°C, 22.5h, 24%.

Table 6. The binding of compound **1** to human MDM2 was characterized by several biochemical methods.

	IC_{50} (nM)	
A: TR-FRET biochem. assay	hMDM2	hMDM4
1	1.7 ± 0.1	2000 ± 300
Nutlin-3a	8.0 ± 1.5	4300 ± 900
B: ITC on hMDM2 [a]		
Kd (nM)	2.3	
ΔH (kcal/mol)	-7.7	
-TΔS (kcal/mol)	-4.1	
ΔG (kcal/mol)	-11.8	
C: DSF on hMDM2		
ΔTm (°C)	25.0	
D: Other PP interactions [b]		
Ras:Raf	4500	
Bcl2:Bak, Bcl2:Bad	>50'000	
Mcl1:Bak, Mcl1:Noxa	>50'000	
XIAP:BIR3, cIAP:BIR3	>50'000	

[a] Stoichiometry = 1. [b] all IC_{50} are expressed in nM and were determined using a TR-FRET assay.

Table 7. In vitro activity of **1** in cellular proliferation assays in human cancer cell lines. Inhibitory effects of **1** on cellular proliferation are expressed as concentration causing 50% growth inhibition (GI_{50}).

Assay	IC_{50} (nM) [a]
GRIP p53 translocation assay	224 ± 45
cell proliferation assays:	
HCT116 (p53$^{WT/WT}$)	454 ± 136
HCT116 (p53$^{-/-}$)	15'983 ± 4'380
selectivity [b]	35
SJSA-1 in SJSA-1 (p53$^{WT/WT}$)	353 ± 190
SAOS2 (p53$^{-/-}$)	20'464 ± 2'377
selectivity [c]	58

[a] Data are shown as mean ± standard deviation from multiple (n=8) independent experiments. [b] Selectivity is determined by the ration of GI_{50} obtained using the HCT-116 p53 null and the HCT-116 p53^{WT} isogenic pair of cell lines. [c] Selectivity is determined by the ratio of GI_{50} obtained using SAOS-2 (p53-null) and SJSA-1 (p53^{WT} and MDM2 amplified) osteosarcoma pair of cell lines.

Figure 5. PK/PD relationship of compound **1** in SJSA-1 tumor-bearing rat. Rat (n=3/time-point) bearing established subcutaneous SJSA-1 xenografts received a single dose of an oral suspension of 30 mg/kg of **1** (compound was suspended in 0.5% HPMC). Levels of **1** were monitored in plasma (red square) at 6 different time-points within 72 h following the dose. As a pharmacodynamic readout, the p53 target genes p21 (green triangle), MDM2 (blue diamond) and PUMA (brown circle) mRNA levels were assessed in the tumor samples by qRT-PCR at 6 time-points within 72 h following single dose of compound **1**. Data are plotted as mean ± SEM.
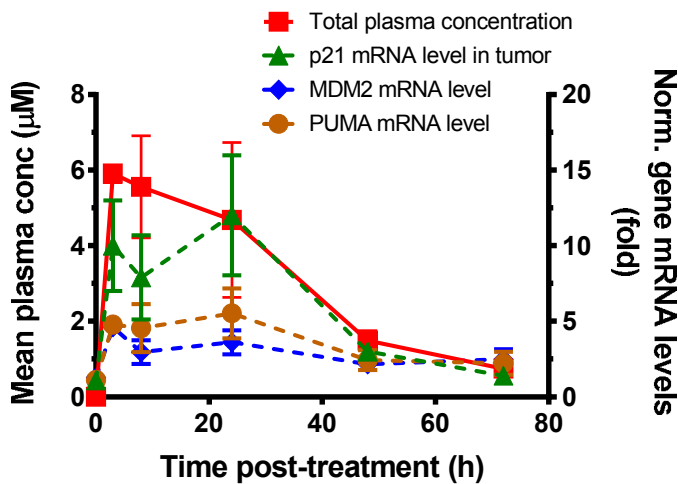
Figure 6. In vivo anti-tumor activity of compound **1**. Rat (n=10/dosing group) bearing established subcutaneous SJSA-1 xenografts received vehicle daily (q24h, black square) or 30 mg/kg daily (orange square) or 3 times a week (3qw, orange triangle) or 70 mg/kg 3 times a week (green triangle) of an oral suspension of **1** (compound was suspended in 0.5% HPMC). Tumor volumes were calipered throughout the study and data are plotted as mean ± SEM (left panel). The body-weight (BW) of the rat was measured three times per week allowing calculation at any particular time-point relative to the day of initiation of treatment (day 0) of the percentage change in BW (%BW). Data are plotted as mean ± SEM (right panel). *, $p < 0.05$ vs. vehicle control.
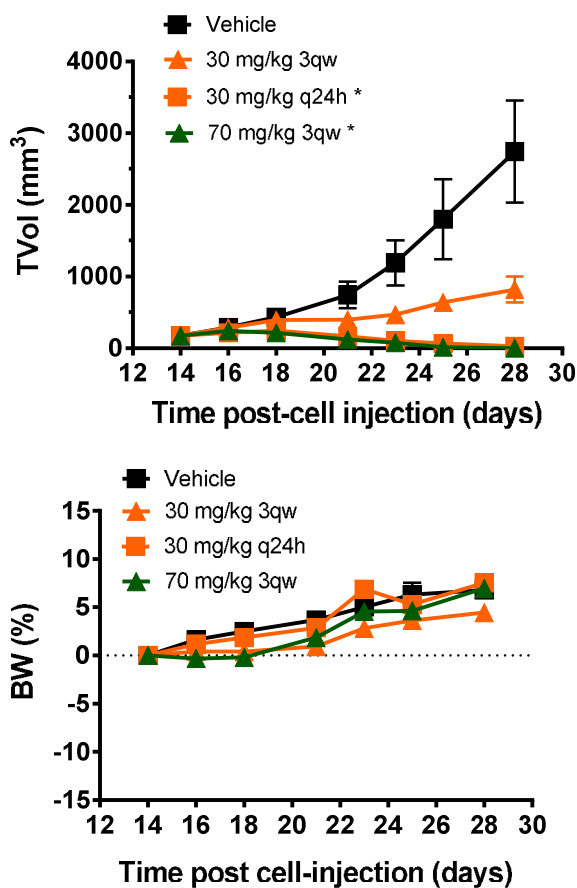
Table 8. Efficacy of compound **1** on MDM2 amplified SJSA-1 tumor model implanted in nude rat. Female athymic rats bearing subcutaneous xenotransplants of SJSA-1 tumors (n=5-12) were treated at 5, 10, 20 or 30 mg/kg or three times a week on Monday, Wednesday and Friday (3qw M, W, F) at 30 or 70 mg/kg p.o. for 14 days. Plasma AUCs were determined at the end of the study. Positive numbers indicate the percentage of tumor growth inhibition (T/C); negative numbers indicate the percentage of tumor regression.

Compound **1** treatment	SJSA-1 model in nude rat			
	T/C or reg (%)	Change in BW (%)	Survival (%)	Plasma AUC_{0-24} (μM.h)
vehicle q24h	-	+1.9/+6.8	12/12	-
5 mg/kg q24h	73	+2.8	6/6	34
10 mg/kg q24h	40	+1.8	6/6	61
20 mg/kg q24h	0.2	+3.4	5/5	163
30 mg/kg q24h	-85*	+4.5	10/10	421
30 mg/kg 3qw	-25*	+4.5	10/10	230 (381)**
70 mg/kg 3qw	-100*	+7.0	10/10	616 (1045)**

* $p < 0.05$ means significantly different from vehicle by using a one way ANOVA (Dunnet's post hoc). ** number in parentheses refer to AUC_{0-48} (μM.h).

Table of Contents Graphic